MEASUREMENT OF THERMAL CHARACTERISTICS OF OFFICE BUILDINGS

L.K. Norford **A. Rabl** **R.H. Socolow** **A.K. Persily, Ph.D.**
ASHRAE Associate Member

ABSTRACT

Thermal characteristics of two adjacent office buildings have been obtained from measurements of temperature, energy consumption and air exchange. The characteristics include the total heat-loss coefficient, a solar aperture, and building heat capacity. The heat-loss coefficient has been determined by steady state and transient analyses; transient analysis is required for the remaining characteristics. The effect of measured infiltration and ventilation rates on the total heat-loss coefficient has been identified. Two methods have been used for the transient analysis: the equivalent thermal parameter method of Sonderegger and the Fourier method of Subbarao.

INTRODUCTION

Two new office buildings in New Jersey have been instrumented to monitor and analyze their energy consumption. Several months of data have been collected, enough to permit a preliminary assessment of the performance of the buildings. The purpose of this paper is to show that thermal characteristics of the buildings can be determined from measurements of temperature, energy consumption, and air exchange. These characteristics include a total heat-loss coefficient, a solar aperture, and a building heat capacity. The determination of these parameters has three major benefits to energy analysts:

1. The data required for the analysis have intrinsic interest. Energy consumption data are the focus of the analyst's activity. Indoor and outdoor temperature data, along with solar radiation measurements, answer questions about occupant comfort: how effectively the HVAC system controls indoor temperature during occupied periods and allows the temperature to float when the building is unoccupied, under a range of weather conditions. Airflow measurements check whether the outdoor airflow into the building meets code requirements and can also quantify the tightness of the building envelope.

2. The thermal parameters could be used in a simple, hourly, microcomputer-based calculation of building energy consumption to predict the effect of retrofit measures (both modifications of building envelope and equipment and modifications of building operation). Such a program would require as inputs a description of the HVAC equipment and building schedules. The characteristics of the building envelope are represented by the thermal parameters, including air exchange rate, rather than by a detailed description of building materials and dimensions.

   An alternate approach to analyzing retrofits is based on such programs as DOE-2 and BLAST. This method requires access to the programs and considerable programming expertise and labor. However, for buildings that have been modeled by one of these programs during the design stage, the input files could be saved and passed on to the building owner, along with the traditional blueprints. This could greatly facilitate the work of the energy auditor by eliminating most of his programming labor. It would also expand the circle of users of these computer programs, with associated economies of scale for the software cost.

L.K. Norford, A. Rabl and R.H. Socolow are with the Center for Energy and Environmental Studies, Princeton University, Princeton, NJ. A.K. Persily is a mechanical engineer at the National Bureau of Standards, Gaithersburg, MD.

3. For those buildings where a prediction of energy use has been made, the experimentally determined thermal characteristics help to reconcile differences between measurement and predictions.

DESCRIPTION OF BUILDINGS

A plan view, Figure 1, shows that each building is aligned in the north-south direction and has a large enclosed atrium with glass facades adjacent to the courtyard that separates the buildings. The interior of each building contains a U-shaped corridor, designed as a light slot with large skylights. The light slots are conditioned, while the atria temperatures are allowed to float. The conditioned floor area of each building is 130,000 ft^2 (12,100 m^2), spread over three stories.

Both buildings are all-electric and have variable-air-volume (VAV) air distribution systems, with central supply and return fans arranged as shown in Figure 2. The south building uses two identical groundwater-coupled heat pumps for heating and cooling. The north building employs electric-resistance heat and uses an ice pond seasonal storage system (Kirkpatrick et al. 1985) with a backup of conventional chillers for cooling.

Two data acquisition systems were used in this study: a permanent system and a semi-portable airflow measuring system described later in this paper. Of particular interest in the former system are the channels for ambient conditions (temperature, solar radiation on horizontal and on vertical facades, wind, humidity), five air temperature sensors in each building, flow and water temperature sensors for the south building heat pumps, and electric meters. The data are collected by a microcomputer at the site and transmitted by modem to an office microcomputer for storage and analysis.

To determine thermal characteristics, one must know how much of the total electricity usage of the buildings contributes to the thermal balance. We have used both electric meters tied to the data acquisition system and a portable electric power meter, and have encountered several problems:

1. In the south building, the electricity used by the chillers must be converted to thermal power, requiring additional computation and the use of sensors inherently less accurate than kWh meters.

2. Electricity metering to date has not isolated the electricity used by the parking lot lights or outdoor floodlights. It also cannot determine the fraction of the atria light energy use contributing to the heat gain of the buildings' conditioned spaces nor the heat gains contributed by the mechanical equipment rooms. Estimates were required in each case.

3. The computer rooms have their own separate cooling systems that exhaust directly to the outside. It is assumed that the extra heat generated by the computers is removed by the local chillers, with negligible heat flow between the computer rooms and the rest of the building. The computers operate continuously and spot readings of computer and local chiller electrical power are considered to be adequate.

THERMAL BEHAVIOR OF THE BUILDINGS

The single most important thermal parameter is the total heat loss coefficient $(UA)_{tot}$, in units of Btu/h·F (kW/C). It is defined by

$$\frac{Q_{net}}{T_{int} - T_{amb}} = (UA)_{tot} = (UA)_{air} + (UA)_{cond} \qquad (1)$$

where

Q_{net} = net thermal power within the building envelope

$(UA)_{air}$ = heat-loss coefficient for air infiltration and ventilation

$(UA)_{cond}$ = heat-loss coefficient for conductive heat transfer through the building envelope

In most cases knowledge of $(UA)_{tot}$ is sufficient for a first order estimate of the annual heating and cooling loads. Corrections due to transient heat flow into and out of the thermal mass of the building tend to be relatively small, often on the order of 10%. But when evaluating the effect of different operating procedures, one is concerned with small changes, and an accurate treatment of transient effects may be essential.

The total heat-loss coefficient can be determined from Equation 1 if one selects time periods for which the initial and final temperatures of the concrete floor slabs (the dominant mass in the buildings) are the same. We use indoor air temperatures as an indication of mass temperature. To identify thermal mass effects one needs data with changing interior temperatures. In the following we report results for both types of analysis.

Steady-State Analysis

For the north building, for which data of higher quality are available, the average conductive term calculated from the steady state energy balance is

$$(UA)_{cond} = 23.1 \text{ kBtu/h·F } (12.2 \text{ kW/C}) \quad (2)$$

as indicated in Table 1. For the south building the value is comparable, although less certain because reliable data are available for only a very short period. Based on the architect's plans, we had calculated a value of 23.1 kBtu/h·F (12.2 kW/C) for the south building, and a similar value for the north building. The $(UA)_{air}$ term varies with the operation of the HVAC system, as shown in Table 1 and presented in more detail later in this paper. The air infiltration/ventilation rate, averaged over the time periods used in the thermal analyses, varied from 0.42 to 1.01 exchanges per hour, where 0.74 exchanges per hour corresponds to 23.1 kBtu/h·F (12.2 kW/C), the average conductive term.

The steady state analysis of south building summer cooling data is shown in graphical form in Figure 3. There is a clear linear trend, but the scatter is large, and the value of $(UA)_{tot}$, 33.9 kBtu/h·F (17.9 kW/C) is very small based on prediction. Both the large scatter and the small $(UA)_{tot}$ reflect a basic shortcoming of the steady state model. Due to the operation of the air dampers the heat loss coefficient during the day is about twice as large as that at night. In summer the ratio of daytime and nighttime temperature differences varies strongly from day to day, sometimes even changing sign; this causes large scatter in the data if one assumes a single constant heat loss coefficient. For the heating data, on the other hand, the nighttime and daytime temperature differences are comparable and a plot of heat loss versus average temperature difference can provide a fairly good estimate of the average heat-loss coefficient.

Additional scatter arises from transients (T_{int} does not return exactly to the initial value at the end of a 24 hour period), from the latent cooling load (which we can only guess because the humidity sensor was not yet operating at the time), from uncertainties about the time-of-day distribution of the electricity input (only the daily total was available), and from variations in solar radiation. The total scatter is not inconsistent with the magnitudes of the individual effects. However, an attempt to identify these effects by means of a steady-state analysis was not successful: for example, the point that lies the furthest above the best-fitted line in Figure 3 is also the day with the lowest solar radiation.

Transient Analysis

The transient analysis is considerably more complicated than that for steady state. We have considered several possible methods:

1. The equivalent thermal parameter method of Sonderegger (1977). In this method the building is approximated by a simple thermal network. The parameters of the network are determined through a least squares fit to the data.

2. The modal analysis of Bacot et al. (1984), which uses an expansion in terms of time constants and eigenvectors.

3. The response factor series (Crawford and Woods 1985). Here the interior temperature at the present time is expressed as a linear combination of past temperatures and energy inputs, and the coefficients are determined through a least squares fit to the data. Alternatively one can fit energy against temperatures. This is an application of response factor series as adapted to buildings by Mitalas and Stephenson (1967).

4. The Fourier analysis of Subbarao and his coworkers (1983). The Fourier method describes a building in terms of complex admittances for the dominant frequencies of the input (i.e. zero frequency and diurnal frequency). Recently Subbarao (1985) has refined this method by combining it with response factor series.

We have used two methods: the equivalent thermal parameter method because it is conceptually the simplest, and the most recent method of Subbarao (1985) because it is general and systematic and yields results having a clear physical interpretation in terms of properties of the building.

Data for the transient analysis must be selected carefully. The air exchange contribution must be either known or constant and interior temperatures must vary significantly to obtain an accurate determination of thermal storage effects. Summer and winter data are preferred because the thermal inputs are large and the air dampers are in fixed positions. For this paper we have used weekend data for the south building, when the heat pumps were not running and outside air intake dampers were closed.

Equivalent thermal parameters. The first step is the selection of the thermal network. In the buildings studied most of the heat capacity lies in the concrete floors; the mass of the walls is outside the insulation and can be considered decoupled from the interior temperature. A thermal resistance couples the floor to the interior air. The simplest network satisfying these requirements, shown in Figure 4, has four parameters: the total heat loss coefficient $(UA)_{tot}$; the effective heat capacity, C (in Btu/F [kWh/C]) of the building mass (Sonderegger 1977); the conductance, $(1/R_C)$, between interior and mass; and the solar aperture A_{sol}, defined by

$$Q_{sol} = A_{sol} H_{sol} \qquad (3)$$

where

Q_{sol} = total solar heat gain, Btu/h (kW)

H_{sol} = solar radiation on a horizontal surface, Btu/h·ft^2 (kW/m^2)

This simple network is too crude to account for all the properties of the building. For example, a single solar aperture relative to horizontal radiation cannot fully describe the variation of the solar heat gain with time of day and year and with the ratio of diffuse and direct insolation, but a more realistic model for the solar gains would contain more parameters than could be meaningfully determined. For a discussion of these questions see Sonderegger (1977), Subbarao (1984) and Norford et al. (1984).

We have fitted both the summer and the winter data to the differential equation for the thermal network of Figure 4, using hourly time steps and taking the future interior temperature as the dependent variable. The results are listed in Table 2 and have rms errors of about 0.5 F (0.3 C). Comparing with the predicted $(UA)_{cond}$ value of 23.1 kBtu/h·F (12.2 kW/C), which is calculated from the building description, we see that the $(UA)_{tot}$ value listed in Table 2 is so low as to leave no room for infiltration. The effective heat capacity for diurnal temperature variations is expected to be about 760 kBtu/F (400 kWh/C); our result of 1330 kBtu/F (700 kWh/C), equal to the total heat capacity of the floor slabs, seems too large because diurnal heat flow does not fully penetrate into the slabs (Carslaw and Jaeger 1959; Sonderegger 1977). The conductance between floor and interior air at the time of this test (unoccupied period, no ventilation, and carpets and ceiling plenum not yet installed in most of the building) is expected to be on the order of 340 kBTU/h F (180 kW/C); the value of 210 kBTU/h·F (111 kW/C) in Table 2 is reasonable.

The solar aperture is found to be 2150 ft^2 (200 m^2), roughly consistent with the preliminary data from April, 1984 (Norford et al. 1984) as well as with the Fourier results reported below. As mentioned above, the concept of an effective solar aperture for buildings is somewhat ill-defined theoretically. According to a theoretical calculation based on window orientations, dimensions, and transmittances, the solar aperture should vary from a low of 4730

ft^2 (440 m^2) in summer to a sharply peaked high of 11,600 ft^2 (1080 m^2) in December (Princeton Energy Group [PEG] 1983). The discrepancy is so large that we measured with a pyranometer the solar radiation actually transmitted by each window. This is a difficult and tedious task: due to the complicated geometry of these buildings the transmitted radiation varies strongly with time and weather. This exercise gave an aperture of 2700 ft^2 (250 m^2), subject to large uncertainty (Protopapas 1985). The situation is further complicated by the fact that the windows have Venetian blinds that can be adjusted by the tenants. The PEG estimate assumed an attenuation factor of 0.6 for the blinds. For the data sets reported here, the second and third floors were unoccupied and without any blinds. The determination of the effective solar aperture of a building can be extremely difficult, and we do not yet have the final answer.

Fourier Method. A good exposition of this subject can be found in the book by Shurcliff (1984)). The Fourier approach is natural because the driving forces (ambient temperatures, solar radiation, and heat input) follow a quasiperiodic pattern of diurnal cycles which results in a diurnal cycle for the response of the building (interior temperature). The heat transfer mechanisms in a building can be approximated very well by linear equations. The response of any linear system to a sine wave input is also a sine wave of the same frequency, and can be characterized by two constants: an amplitude and a phase. To a good approximation only two frequencies are relevant for most buildings: the zero frequency or steady state, and the diurnal frequency. No phase change occurs for the zero frequency case and therefore three parameters per driving force should be sufficient to describe the response of a building. With the typical three driving forces of ambient temperature, solar radiation and thermal input (from heating/cooling equipment, lights, and occupants) this leads to nine parameters. Two of these turn out to be identical, and so the number of independent parameters is only eight.

The parameters can be stated in terms of admittances: V for interior temperature, W for ambient temperature and S for solar radiation. At zero frequency

$$V_0 = W_0 = (UA)_{tot} \tag{4}$$

$$S_0 = A_{sol} \tag{5}$$

The admittances for the diurnal frequencies are complex, and an interpretation will be given below.

The method of Subbarao (1985) begins by determining the coefficients of the response factor series through a least-squares fit to the data. Then the complex admittances of the building are calculated as the Fourier transform of these coefficients. Strictly speaking, one needs an infinite number of terms for the Fourier series, but in practice the admittances converge rapidly to their correct values and one can obtain good results with as few as two terms for each admittance. The final result is the set of eight numbers that specify the admittances at zero and at diurnal frequency. Subbarao removes the shortcomings of the response factor series method: coefficients which lack clear physical significance and which can change drastically as new coefficients are added (Subbarao 1985). Subbarao also provides a solution to the problem of deciding how many parameters to use for the data fit. This is a serious difficulty with the thermal network approach, where there is no systematic procedure for adding terms to improve the accuracy of a fit.

The results of the Fourier method are listed in Table 3. The steady-state parameters are close to the thermal network numbers. The conductance, $(UA)_{tot}$ = 26.0 kBtu/h-F (13.7 kW/C), is high enough to accommodate air infiltration of about 0.1 air change per hour, quite plausible for summer conditions with their small temperature differences and wind speeds (see Figures 6 and 7).

The admittances for diurnal frequency are stated in terms of absolute value and phase. They determine the magnitude and time lag of the response of interior temperature or heating/cooling load to sinusoidal variations of ambient temperature or solar radiation. Suppose, for example, that the driving forces are constant except for the ambient temperature, which varies about its average value according to

$$T_{amb}(t) = \Delta T_{amb} \cos (2 \pi f t) \tag{6}$$

where

t = time of day,

ΔT_{amb} = amplitude of variation of ambient temperature

f = diurnal frequency = 1/24 hr.

Then the interior temperature varies about its average value according to

$$T_{int} = \frac{|W_1|}{|V_1|} \Delta T_{amb} \cos [2 \pi f t - (\phi_V - \phi_W)] \quad (7)$$

where

$|W_1|$ and ϕ_W are the amplitude and phase of the admittance of T_{amb} at the diurnal frequency

$|V_1|$ and ϕ_V are the amplitude and phase of the admittance of T_{int} at the diurnal frequency

From Table 3,

$$\frac{|W_1|}{|V_1|} = 0.087 \quad \text{and} \quad \phi_V - \phi_W = 34.8 \text{ degrees} = 2.3 \text{ hr} \quad (8)$$

This means that an ambient temperature variation of ΔT_{amb} = 1.8 F (1 C) causes an interior temperature variation of 0.157 F (0.087 C) with a time lag of 2.3 hours.

Similarly, for the solar radiation, Table 3 shows that

$$\frac{|S_1|}{|V1|} = 5.50 \text{ ft}^2 \text{ F·h/kBtu } (0.97 \text{ m}^2\text{C/kW}) \text{ and}$$

$$\phi_V - \phi_S = 69.9 \text{ degrees} = 4.7 \text{ hr} \quad (9)$$

For a sunny summer day in New Jersey the amplitude of the solar variation delta H_{sol} is on the order of 0.13 kBtu/h·ft^2 (0.4 kW/m^2); it causes an interior temperature variation with amplitude 0.7 F (0.4 kW/m^2 * 0.97 C m^{2}C/kW = 0.4 C) which peaks 4.7 hours after noon.

In general, several driving forces contribute together and the individual sine wave contributions are added to find the total amplitude and phase of the interior temperature. For instance, on Sunday, July 8, 1984, the only variable inputs were ambient temperature and solar radiation. The data, shown in Figure 5, give the following information about the amplitudes and phases:

ΔT_{amb} = 11.0 F (6.1 C) with peak at 3.5 hours after noon

ΔH_{sol} = 0.16 kBtu/ft^2 (0.50 kW/m^2) (a very sunny day) with peak at 1.0 hours after noon (daylight saving time; correction for longitude and solar equation of time is only four minutes (see, e.g., Rabl 1985).

The resulting contributions to the interior temperature variation are from ambient temperature:

amplitude 0.95 F (6.1 * 0.087 C = 0.53 C)

with peak at 3.5 + 2.3 = 5.7 hours after noon

and from solar radiation:

amplitude 0.88 F (0.50 * 0.97 C = 0.49 C)

with peak at 1.0 + 4.7 = 5.7 hours after noon.

The peaks are so close together as to be practically in phase, and we can simply add the amplitudes to find a total ΔT_{int} = 1.83 F (1.02 C) with peak at 12.0 + 5.7 = 17.7 hours. This agrees quite well with the amplitude of 2.2 F (1.2 C) and peak at 18.5 hours that were actually observed on this day.

As a test of the results of the transient analysis, regardless of the choice of model, one can calculate the interior temperature in an hour-by-hour simulation, with the model parameters determined from the data. Inputs for this simulation are the measured values of ambient temperature and solar radiation and the initial value of the interior temperature, as well as data for any additional energy flow into the building. Figure 5 shows such a fit based on the thermal network parameters of Table 2. Only daily electric consumption was available; because the building was unoccupied and HVAC equipment was not running, we assumed a constant hourly rate (82 kBtu/h [24 kW]). The agreement between calculated and measured interior temperatures is good, considering the quality of the data; for our fits in general we have found that the rms deviation between measured and calculated interior temperatures is on the order of 0.5 F (0.3 C).

INFILTRATION AND VENTILATION MEASUREMENTS

Measuring Technique

The tracer gas tests included decay measurements of the buildings' infiltration and ventilation rates and whole building pressurization tests of the buildings' airtightness. Both kinds of measurements were made with a microcomputer-controlled system (Grot 1982).

In the tracer gas decay tests, a small amount of sulfur hexafluoride (SF_6) was released into the two supply ducts in each building every three hours. The tracer gas was then allowed to mix with the interior air until the SF_6 concentration became uniform throughout the building. At this point the decay in tracer concentration was monitored. The negative of the decay rate of the natural logarithm of the concentration is equal to the air change rate of the building in units of building volumes or exchanges per unit of time. The results of the measurements are hourly average infiltration and ventilation rates. Tests were conducted for several hundred hours to study the effects of inside-outside temperature difference and wind speed rates.

The ventilation rate was measured with the building HVAC system operating normally under occupied conditions: spill and intake dampers open and close as the control system dictates. Infiltration refers to uncontrolled air leakage through the building envelope: the measurements were made with the spill and intake dampers closed (including minimum outside air dampers), all local exhausts off, and the air handlers running, and the test results provide an indication of the airtightness of the building envelope.

The whole building pressurization tests are a one-time measurement of the airtightness of the building envelopes, requiring several hours. A fan induces a large and uniform pressure difference across the building envelope, and the airflow rate required to induce the pressure difference is measured (Grot et al. 1985). Several inside-outside pressure differences are generally induced during such a test. The airflow rate associated with a specific pressure difference serves as a measure of the airtightness of the building envelope. Because the test conditions are considerably different than those normally encountered by the building, it is not clear how the results of such a pressure test relate to a building's infiltration rate under normal conditions.

In our tests, the buildings' air-handling equipment induces the test pressure differences, and a constant injection tracer gas method measures the airflow rates (Lagus and Persily 1985). The supply fans operate, with all return and exhaust fans off. All return and spill dampers are closed and supply air flowing into the building can leave only through the outside doors, windows, and other leakage sites. To measure the airflow rate, SF_6 is injected at a constant and known rate into the supply airstream at a location close to the outside air intake vent. The tracer gas concentration is measured in the supply duct, far downstream from the injection point. Under conditions of good mixing of the tracer gas with the airstream, the airflow rate can be determined from the SF_6 injection rate and the measured concentration. The airflow rates into the buildings were modulated by adjusting the inlet vanes on the supply fans. For each data point, the inside-outside pressure difference was measured at several locations over the building envelope using magnetic linkage type, differential pressure gauges.

RESULTS

Infiltration. Hourly average infiltration rates are plotted against the inside-outside temperature difference in Figure 6 (north building) and Figure 7 (south building). In both buildings the infiltration rate increases with temperature difference. Such a temperature dependence has been observed in other large office buildings (Grot et al. 1985), and the subject buildings exhibit a relatively strong dependence compared to the other buildings. The infiltration data collected to date in the buildings shows no dependence on wind speed. Some previously monitored office buildings have exhibited some dependence of infiltration on wind speed, although a wind dependence is less common than a temperature effect.

One difficulty with the infiltration measurements lies in the need to run the fans in order to insure that the air inside the building is well mixed. Because the fans are designed to pressurize the building, with the supply flow rate controlled to exceed the return flow rate by 20,000 cfm (9400 L/s), the supply fan will bring in air across the somewhat leaky outdoor air dampers. The measured air infiltration rate will therefore overestimate the true value. This problem can be avoided by adjusting the fan controls to eliminate the difference between supply and return air flows, a step which the building operator preferred not to take.

Ventilation. The measured ventilation rates include both intentional outside air intake through the air handlers and unintentional air leakage through the building envelopes. Studies of other modern office buildings have revealed that these two quantities are often comparable in magnitude (Grot et al. 1985). Ventilation data are plotted against inside-outside temperature difference in Figure 8 (north building) and Figure 9 (south building). The data in these two plots exhibit a great deal of scatter, but some features are worth noting. First, in both buildings there is a minimum ventilation rate. This minimum is due to the outside air intake through the minimum outside air dampers, which is required to maintain acceptable indoor air quality. This measured minimum also includes air leakage through the building envelopes. The ventilation rates measured during the first fall of operation correspond to the open circles in the graphs. These ventilation rates tend to be lower than the rates measured later on. During this period the air-handling equipment and control system were in the process of "debugging," and the minimum ventilation rates were less than their design value.

Previous ventilation measurements in modern office buildings have exhibited stronger dependences on temperature difference than is observed here (Persily and Grot 1985). In the earlier studies, the ventilation rates were generally at a minimum during hot and cold weather conditions in order to minimize the space conditioning load. During mild weather, outside air was used to condition the buildings and large ventilation rates were induced. Such a pattern is not evident in either building, probably due to the continuing adjustments of the air-handling equipment and controls during the first year of operation. The north building would exhibit the expected pattern if the summer ventilation rates were lower. The air exchange rate in both buildings shows large peaks even in winter, as plotted in Figures 10 and 11, as the flow rate of air supplied to the offices increases and more outdoor air is brought in to maintain a fixed supply air temperature.

The earlier ventilation measurements in large office buildings also revealed that the net ventilation rates were less than that recommended by ASHRAE Standard 62-1981 (ASHRAE 1981, Persily and Grot 1985). Neglecting the measurements from the first fall of building operation, both of the subject buildings have minimum ventilation rates of about 0.6 exchanges per hour. One can convert the ASHRAE ventilation recommendation of 20 cfm (10 L/s) per person when smokers are present to air exchanges per hour by assuming an occupant density of seven people per 1000 ft^2 (100 m^2) and a ceiling of 13 ft (4 m), including the return plenum. This translates to an air exchange rate of 0.65 exchanges per hour. Therefore both buildings are essentially in compliance with the ASHRAE recommendations.

Pressurization. The south building was pressurized with the supply air fans to five different inside-outside pressure differences Δp: 0.049, 0.093, 0.133, 0.170, and 0.205 in H_2O (12.3, 23.3, 33.3, 42.5, and 51.3 Pa). At each pressure difference, the airflow rate, Q, required to induce and sustain the interior pressure at this elevated level was measured using the constant injection tracer gas procedure described earlier. The data were fit to a curve of the form:

$$Q\ (cfm) = 2.37 \times 10^5 \quad \Delta p^{.801} \qquad (10)$$

In previous applications of whole building pressurization testing to large commercial buildings, the airflow rate at 0.1 in H_2O (25 Pa), based on a curve fit of the form shown in Equation 10, served as a measure of the building airtightness (Grot et al 1985). For the south building, this airflow rate equals 3.74×10^4 cfm (1.76×10^4 L/s). One can normalize this value by the building volume, to obtain 1.35 exchanges per hour. Alternatively, normalizing by the building surface area, one obtains 0.441 cfm/ft^2 (2.24 L/s-m^2). Previous results for modern U.S. office buildings ranged from 0.5 to 1.5 exchanges per hour and from 0.1 to 0.5 cfm per ft^2 of envelope area (0.5 to 2.5 L/s-m^2) (Grot et al. 1985). Thus, the south building is leakier than average in terms of both exchanges per hour and airflow rate per unit envelope area. Exchanges per hour are more closely related to naturally induced infiltration rates, while the airflow rate divided by envelope area is more of a measure of construction quality.

CONCLUSION

With measurements of air temperatures and building internal heat generation, the total heat-loss coefficient of a building can be accurately determined. Airflow measurements can be used to separate the heat-loss coefficient into conduction and infiltration/ventilation terms. For the two buildings, the airflow data show a strong dependence of infiltration on indoor-outdoor temperature difference. The minimum ventilation rate is in compliance with ASHRAE Standard 62-1981. Pressurization test results indicate that the south building envelope is relatively leaky when compared to other buildings.

With the addition of solar radiation data a transient analysis can be performed to determine a solar aperture and heat capacity effects. Air exchange data are essential, because the variation of the exchange rate causes large variations in the total heat-loss coefficient of the building. In this paper both the thermal network method and the Fourier method have been used for the transient analysis. Both methods permit the development of models that can reproduce the temperature of the building with good accuracy (rms error less than 0.5 F (0.3 C)). However, some of the parameters found for the thermal network differ appreciably from theoretical expectations, probably due to the fact that the network is unrealistically simple. The results of the Fourier analysis look very reasonable.

REFERENCES

ASHRAE. 1981. ASHRAE Standard 62-1981, "Ventilation for acceptable indoor air quality." Atlanta: American Society of Heating, Refrigerating and Air-Conditioning Engineers, Inc.

Bacot, P.; Neveu, A.; and Sicard, J. 1984. "Analyse modale des phenomenes thermiques en regime variable dans le batiment." Revue Generale de Thermique, No. 267, p.189, March.

Carslaw, H.S.; and Jaeger, J.C. 1959. Conduction of Heat in Solids. 2d ed. London: Oxford University Press.

Crawford, R.R.; and Woods, J.E. 1985. "A method for deriving a dynamic system model from actual building performance data." ASHRAE Transactions, Vol. 91, Part 2.

Grot, R.A. 1982. "The air infiltration and ventilation rates in two large commercial buildings." Proceedings of DOE/ASHRAE conference, Thermal Performance of the Exterior Envelopes of Buildings II, Las Vegas, NV, ASHRAE SP 38.

Grot, R.A.; Persily, A.K.; Chang, Y.M.; Fang, J.B.; Weber, S.; and Galowin, L.S. 1985. "Evaluation of the thermal integrity of the building envelopes of eight federal office buildings." National Bureau of Standards report NBSIR 85-3147.

Kirkpatrick, D.L.; Masoero, M.; Rabl, A.; Roedder, C.E.; Socolow R.H.; and Taylor, T.B. 1985. "The ice pond: production and seasonal storage of ice for cooling." Solar Energy, Vol. 35, Number 5. See also Princeton University/Center for Energy and Environmental Studies reports PU/CEES 149 (long version) and 149a (short version).

Lagus, P.; and Persily, A.K. 1985. "A review of tracer-gas techniques for measuring airflows in buildings." ASHRAE Transactions, Vol. 91, Part 2.

Norford, L.K.; Rabl, A.; Ryan, L.E.; and Socolow, R.H. 1984. "Measuring solar gains of office buildings." Proceedings of the American Council for an Energy-Efficient Economy's Summer Study, Santa Cruz, CA, August.

Princeton Energy Group. 1983. Summary report on analysis of Enerplex.

Persily, A.K.; and Grot, R.A. 1985. "Ventilation measurements in large office buildings." ASHRAE Transactions, Vol. 91, Part 2.

Protopapas, A. 1985. "Solar gains: a study of the Enerplex south building." Junior thesis, Dept. of Chemical Eng. Princeton University. May.

Rabl, A. 1985. Active solar collectors and their applications. New York: Oxford University Press.

Shurcliff, W. A. 1984. Frequency method of analyzing a building's dynamic thermal performance. Publ. by Shurcliff, 19 Appleton St., Cambridge, MA 02138.

Sonderegger, R. C. 1977. "Modeling residential heat load from experimental data: the equivalent thermal parameters of a house." Proceedings of the International Conference on Energy Use Management. Tucson, AZ. Pergamon Press.

Stephenson, D.G.; and Mitalas, G.P. 1967. "Cooling load calculations by thermal response factor method." ASHRAE Transactions, Vol. 73, Part 1.

Subbarao, K. 1985. "Thermal parameters for single and multizone buildings and their determination from performance data". Solar Energy Research Institute report SERI/TR-253-2617. January.

Subbarao, K.; and Anderson, J. 1983. "A graphical method for passive building energy analysis." ASME J. of Solar Energy Engineering, Vol. 107.

ACKNOWLEDGMENTS

The infiltration and ventilation measurements were conducted by the National Bureau of Standards under contract with the U.S. Department of Energy. The remainder of the work was supported by the Prudential Insurance Company. We are grateful for stimulating discussions with Kris Subbarao, and for data fits performed by him as well as by John DeCicco.

TABLE 1

Steady-State Measurements of Heat-Loss Coeficient

time 1985	average values ΔT	ach	Q_{net}	$(UA)_{tot}$	$(UA)_{cond}$
	F (C)	h^{-1}	kBtu/h (kW)	kBtu/h·F (kW/C)	kBtu/h·F (kW/C)
			north building		
			1 ach = 28.6 kBtu/h·F (15.1 kW/C)		
1/18-24	75.7 (24.3)	.78	1940 (570)	44.4 (23.4)	22.0 (11.6)
1/24-30	70.5 (21.4)	.87	1780 (520)	46.2 (24.4)	21.5 (11.3)
1/30-2/1	67.6 (19.8)	.97	1820 (530)	50.8 (26.8)	23.0 (12.2)
2/1-6	75.0 (23.9)	.55	1710 (500)	39.6 (20.9)	23.7 (12.5)
2/7-8	79.2 (26.2)	.76	2130 (620)	45.1 (23.8)	23.5 (12.4)
2/8-9	77.7 (25.4)	.73	2090 (610)	45.8 (24.2)	24.8 (13.1)
			average		23.1 (12.2)
			south building		
			1 ach = 29.6 kBtu/h·F (15.6 kW/C)		
1/18	74.8 (23.8)	1.24	2550 (750)	59.5 (31.4)	22.8 (12.1)

ΔT = $T_{int} - T_{amb}$
ach = air changes per hour
Q_{net} = net heat input

Errors: Uncertainty of 0.1 ach causes 2.9 kBtu/h·F (1.5 kW/C) error in $(UA)_{cond}$. Uncertainties in ΔT and Q_{net} are small, causing errors less than 5 % in $(UA)_{cond}$.

TABLE 2

Results of Thermal Network Method for Unoccupied South Building
Summer Data

parameter	value	estimate
$(UA)_{tot}$	22.7 kBtu/h·F (12.0 kW/C)	23.1 kBtu/h·F (12.2 kW/C) = $(UA)_{cond}$
C	1330 kBtu/F (700 kWh/C)	760 kBtu/F (400 kWh/C)
$1/R_c$	210 kBtu/h·F (111 kW/C)	340 kBtu/h·F (180 kW/C)
A_{sol}	2150 ft^2 (200 m^2)	2700 ft^2 (250 m^2) = independent measurement

TABLE 3

Results of Fourier Method for Unoccupied South Building Summer Data

steady state parameters

$W_0 = V_0 = (UA)_{tot}$ = 26.0 kBtu/h·F (13.7 kW/C)

$S_0 = A_{sol}$ = 2740 ft^2 (240 m^2)

diurnal frequency parameters

admittance for interior temperature

amplitude V_1 = 484 kBtu/h·F (255 kW/C)
phase ϕ_V = 79.5 degrees

admittance for ambient temperature

amplitude W_1 = 42 kBtu/h·F (22 kW/C)
phase ϕ_W = 44.7 degrees

admittance for solar radiation

amplitude S_1 = 2670 ft^2 (248 m^2)
phase ϕ_S = 9.6 degrees

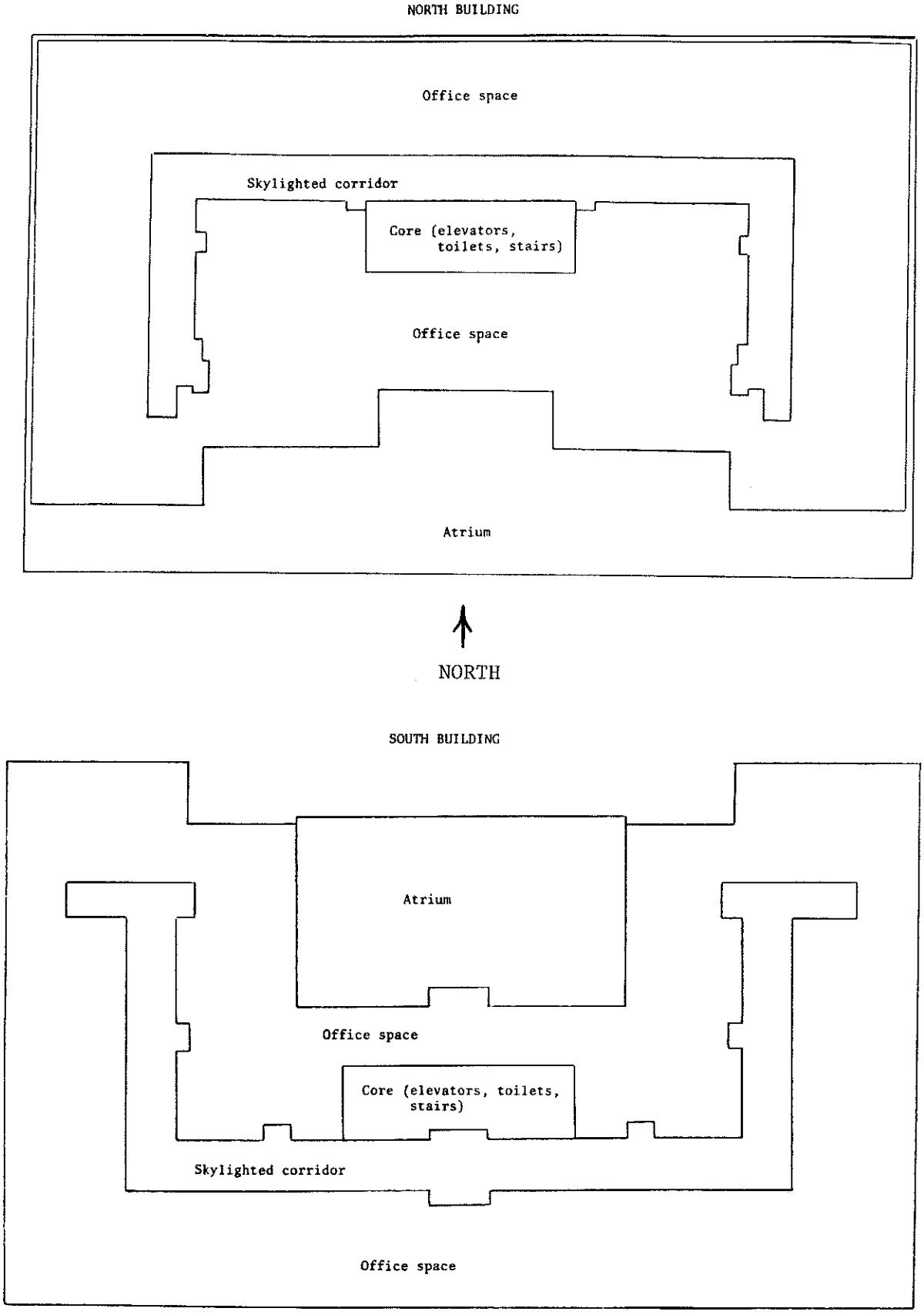

Figure 1. Plan view of buildings, both of which are three stories. The south building facade is of glass and limestone; the north building has an outer glass wall and an inner, partially glazed wall. Sensors for interior temperatures, T, and humidity, H, are on the second floor at the locations indicated

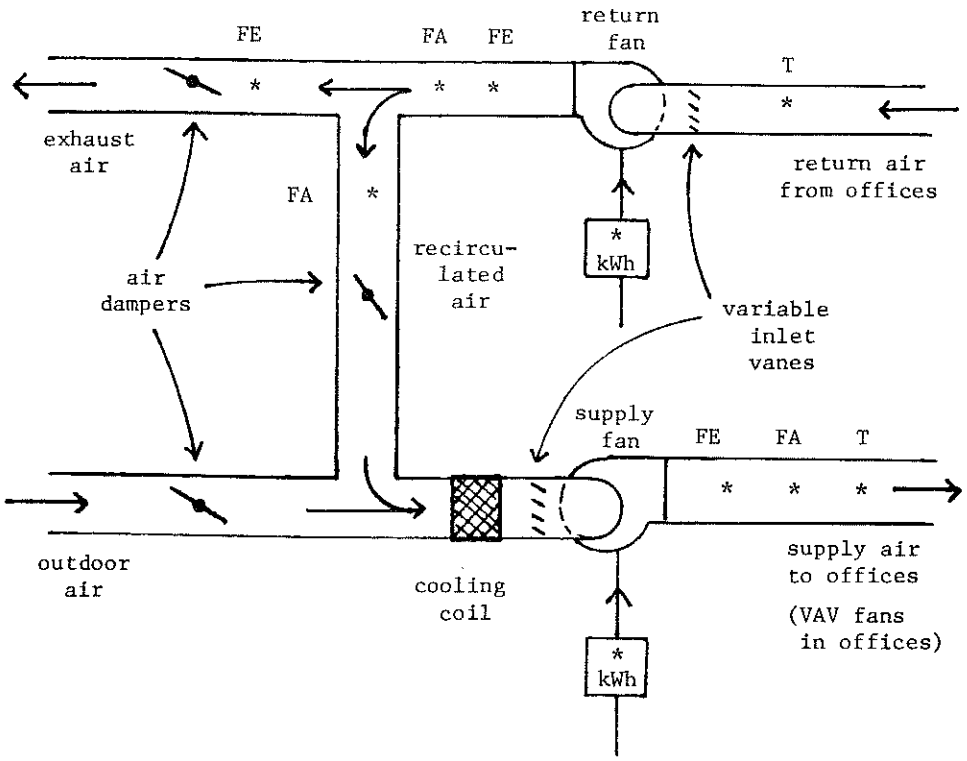

Figure 2. Schematic of ventilation sytem, including location of sensors for temperature, T, airflow (FA for spot anemometer and FE for thermistor averaging meter) and electricity (kWh)

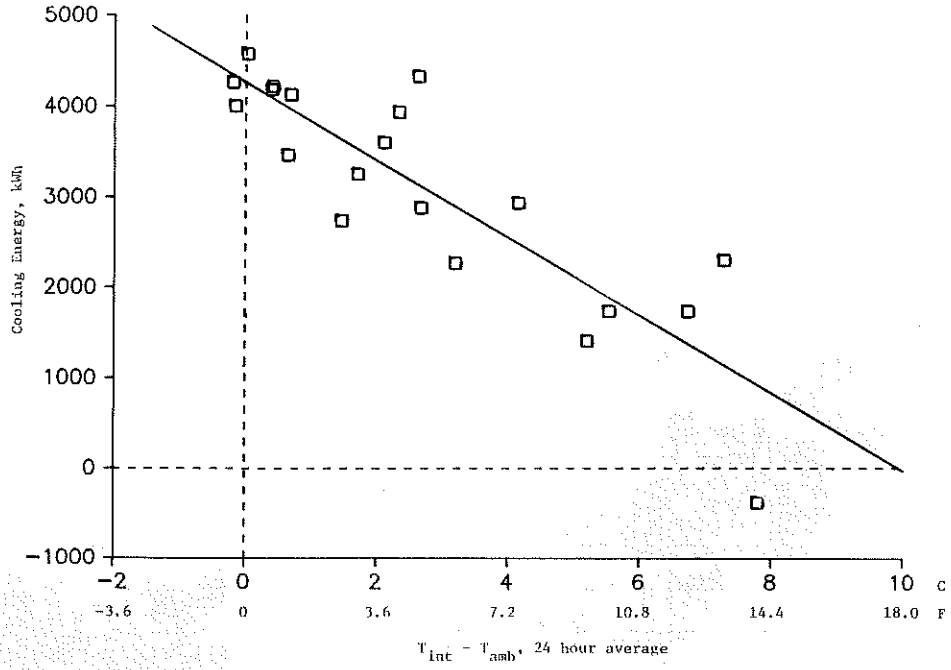

Figure 3. Cooling energy vs. temperature difference. Y-axis shows net cooling energy input to building = total cooling from chillers - electricity for fans, services, lights, and office equipment. Solid line is least squares fit to data. The slope of the best-fit line yields daily cooling energy per degree indoor-outdoor temperature difference; divided by 24 hours, the slope equals $(UA)_{tot}$.

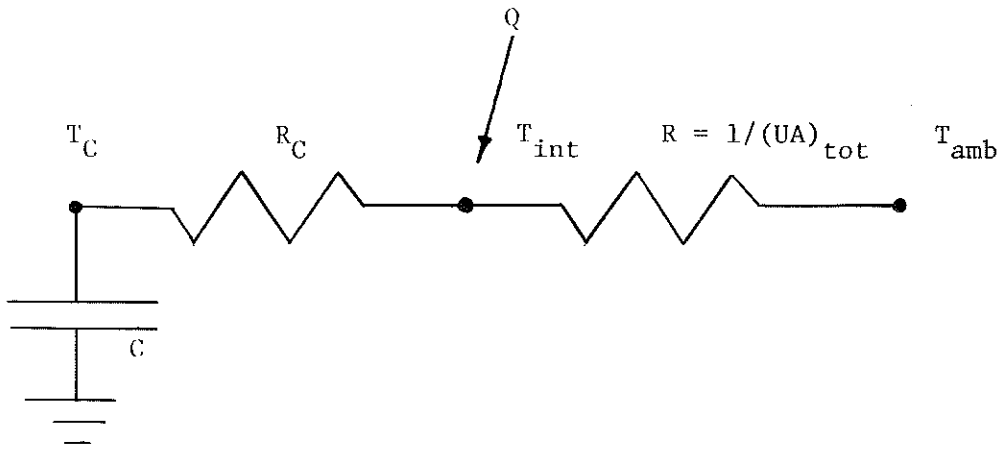

Figure 4. Thermal network used for transient analysis. The capacitance, C, represents the thermal mass of the building, concentrated in the concrete floor slabs and separated from the interior air temperature by thermal resistance, R_C. Heat input, Q, to the interior temperature node is the sum of internal and solar heat gains, where Q_{sol} is the product solar aperture, A_{sol}, and the total horizontal insolation, H_{sol}. The differential equation for this model is

$$\frac{R_C + R}{R} \frac{d\,T_{int}}{dt} = Q + \frac{T_{amb} - T_{int}}{R} + \frac{C\,R_C}{R} \frac{d\,T_{amb}}{dt} - R\,\frac{d\,Q}{dt}$$

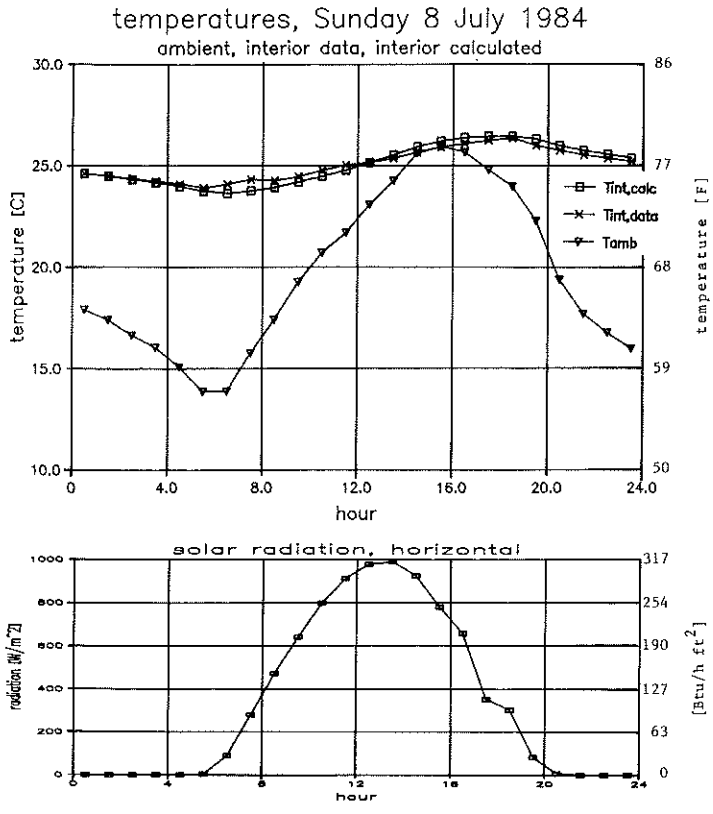

Figure 5. Comparison of interior temperature as measured and as calculated using hour-by-hour simulation with thermal network of Figure 4 and Table 2, for Sunday, July 8, 1984

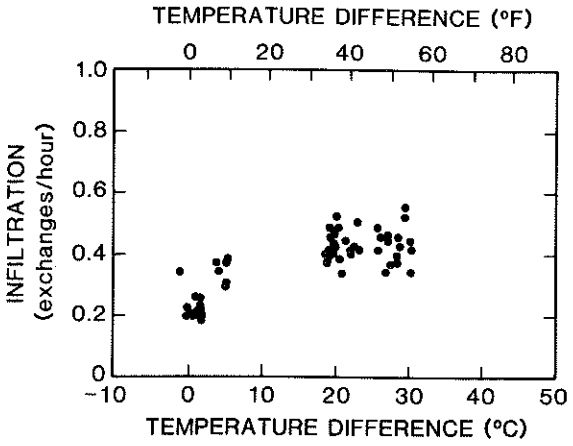

Figure 6. Air infiltration data for north building

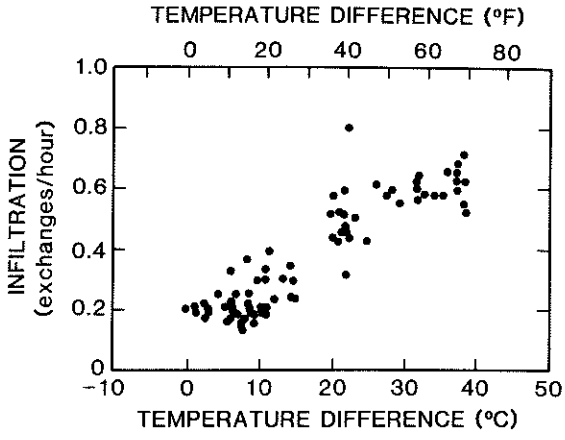

Figure 7. Air infiltration data for south building

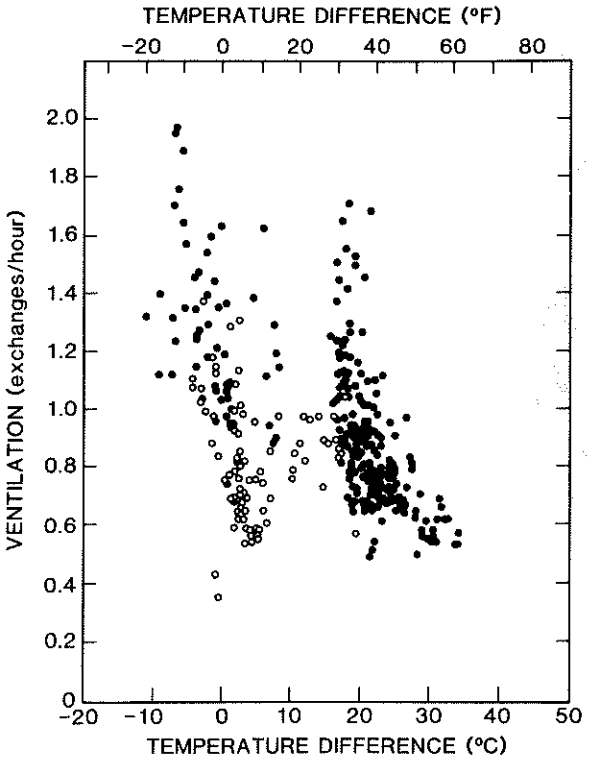

Figure 8. Ventilation data for north building. Open circles indicate measurements made early in building shakedown period

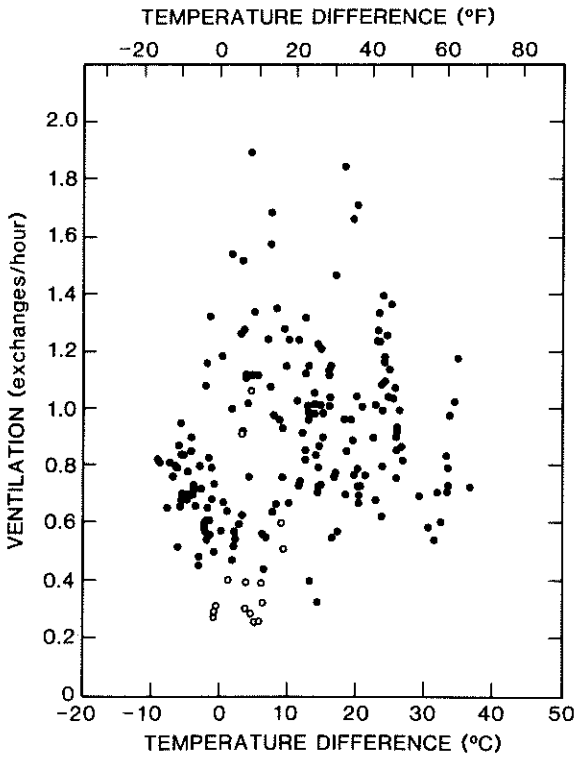

Figure 9. Ventilation data for south building. Open circles indicate measurements made early in building shakedown period

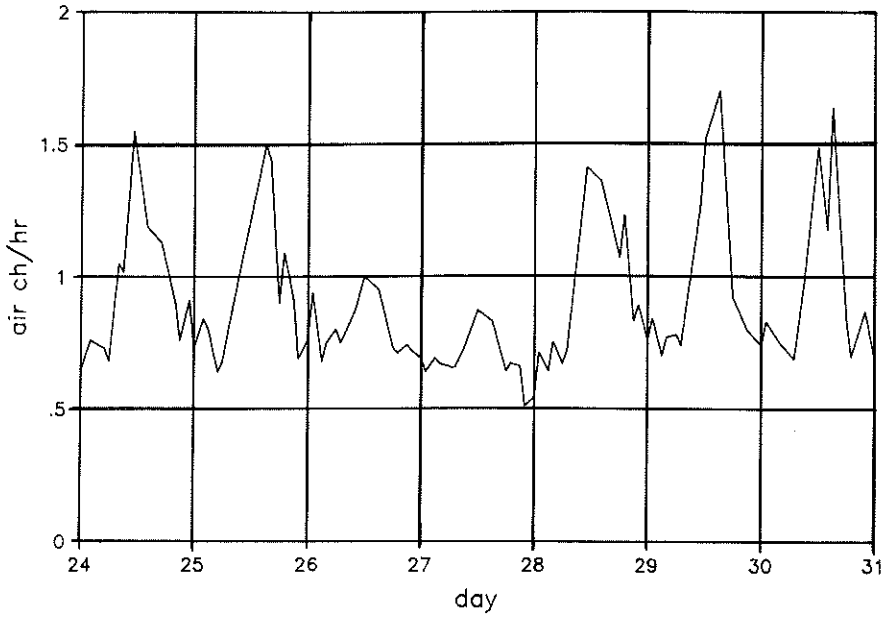

Figure 10. Air exchange vs. time for north building, January 24-31, 1985. Outdoor air intake dampers are open throughout this period. January 26-27 is a weekend. The peaks in air exchange rate are due to the HVAC controls that modulate the outdoor air intake dampers to maintain a fixed supply-air temperature. Outdoor temperatures varied from approximately 19 to 45 F (-7 to 7°C)

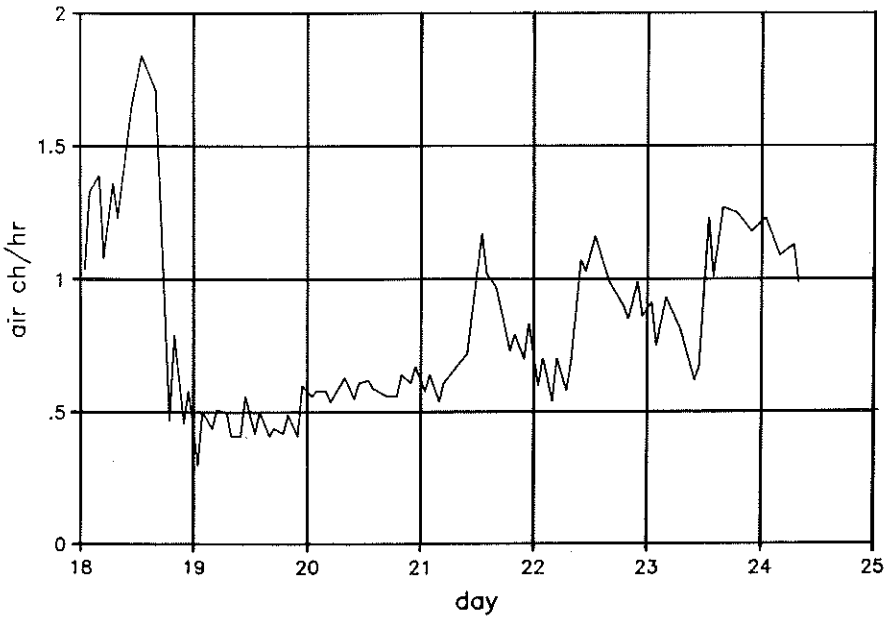

Figure 11. Air exchange vs. time for south building, January 18-24, 1985. Outdoor air intake dampers are closed from 1800, Friday, January 18, through 1000 Monday, January 21; air exchange over this period represents infiltration. Peaks in ventilation rate are due to the HVAC controls, as in the north building. Outdoor temperatures varied from -4 to 37 F (-20 to 3°C)